Absolute differential cross sections for small-angle elastic scattering in helium–rare-gas collisions at keV energies

R. S. Gao, L. K. Johnson, D. E. Nitz,* K. A. Smith, and R. F. Stebbings
Department of Physics, Department of Space Physics and Astronomy, and Rice Quantum Institute, Rice University, Post Office Box 1892, Houston, Texas 77251
(Received 16 March 1987)

This paper reports measurements of absolute differential cross sections for elastic scattering of 0.5-, 1.5-, and 5.0-keV He atoms by Ne, Ar, Kr, and Xe at laboratory scattering angles between 0.05° and 0.5°. Comparisons are made between the measured differential cross sections and those calculated from various model potentials. These comparisons reveal the range of validity of potentials appearing in the literature and provide new information about the lower repulsive walls of the ground-state He–rare-gas interaction potentials.

I. INTRODUCTION

Perhaps the most compelling reason to study differential scattering in atom-atom collisions is to gain information about the interaction potential between the colliding particles. Depending upon the energy and angular range of the measurements, different regions of the interaction potential are probed. Neutral-atom scattering at reduced scattering angles below 1 keV degree is not expected to involve excited states of the collision complex; therefore, such measurements permit study of the ground-state potential alone.

Recent measurements in this laboratory of differential cross sections (DCS's) for He-He elastic scattering[1] have distinguished between several proposed He-He interaction potentials. This paper reports the measurement of absolute cross sections, differential in angle, for scattering of keV-energy, ground-state He atoms by Ne, Ar, Kr, and Xe over a laboratory-frame angular range of 0.05°–0.5°. While thermal-energy and high-energy collisions probe the attractive and higher repulsive regions of the potential surface, respectively, the present work at very small scattering angles and intermediate energies provides information about the lower repulsive walls of the He–rare-gas interaction potentials.

The experiment is based on the technique previously used by Newman *et al.*,[2] in which a well-collimated neutral beam passes through a cell filled with target gas. An axially located, position-sensitive detector (PSD) registers both primary and scattered atoms over the entire angular range of interest. The experimental data are compared with theoretical cross sections obtained from partial-wave calculations using semiclassical phase shifts[3] determined from proposed interaction potentials.[4]

II. APPARATUS AND EXPERIMENTAL METHOD

Figure 1 shows a schematic of the apparatus. Helium ions emerging from an ion source are accelerated to the desired energy and focused by an electrostatic lens. The resulting beam is momentum analyzed and passes through a helium-filled charge-transfer cell (CTC), in which about 10% of the fast helium ions are converted into fast neutral atoms via resonant charge exchange. Deflection plates DP1 remove residual ions from the beam emerging from the CTC.

The exit aperture of the CTC and the entrance aperture of the target cell (TC) are 20 and 30 μm in diameter, respectively, and are separated by 49 cm. The neutral beam is thus collimated to less than 0.003° divergence. The resonant nature of the He^+-He charge exchange occurring in the CTC ensures that essentially all atoms entering the TC are in the ground state.[1,2] The TC is 3.65 mm in length and has an exit aperture 300 μm in diameter. Deflection plates DP2 remove charged collision products from the beam.

Both primary and scattered helium atoms are detected by the PSD, which has an active area 2.5 cm in diameter and is situated 109 cm beyond the TC on the beam axis. The maximum observable scattering angle is thus limited to about 0.7°. The characteristics of the PSD and its application to scattering experiments have been described in detail by Gao *et al.*[5] and by Newman *et al.*[2] An LSI 11/2 microcomputer monitors the output of the PSD electronics and sorts the detected particles into a 90×90 array according to their arrival positions. The bin dimension of the array can be chosen so that it corresponds to a distance on the PSD of 273.6 or 68.4 μm, depending on the angular resolution desired.

For thin target conditions, the differential cross section, $d\sigma(\theta)/d\Omega$ is related to the measured quantities by

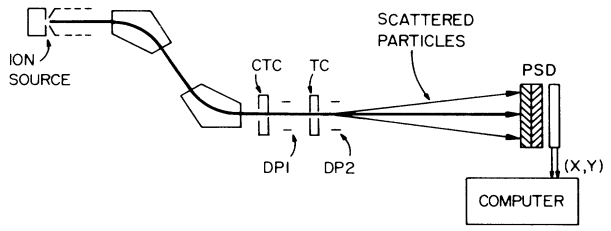

FIG. 1. Schematic of the apparatus.

TABLE I. Experimental uncertainties.

Experimental quantity	Uncertainty contributed to $\frac{d\sigma}{d\Omega}$
Scattered signal, $\Delta S(\theta)$	
Counting statistics	3–15%
PSD operating point	4%
Primary beam flux, S	3%
Density, n	
Pressure measurement and drift	2%
Thermal transpiration correction	2%
Target cell length, L	2%
Solid angle, $\Delta\Omega$	
PSD calibration	4%
TC-PSD distance	2%

the expression

$$\frac{d\sigma(\theta)}{d\Omega}=\frac{\Delta S(\theta)}{S\tau\Delta\Omega},$$

where S is the primary beam flux, $\Delta S(\theta)$ is the flux scattered at angle θ into a solid angle $\Delta\Omega$, and τ is the "target thickness." Recent studies in this laboratory by Newman *et al.*[2] have demonstrated that for the cell used in this experiment, τ is accurately given by the product nL, where L is the physical length of the cell and n is the number density obtained from a measurement of the gas pressure in the TC at a location far from the exit aperture. The pressure is measured using an MKS Baratron capacitance manometer and is corrected for thermal transpiration.[2]

A detailed description of the data acquisition and

TABLE II. Laboratory frame differential cross sections, $d\sigma(\theta)/d\Omega$, for He + Ne collisions, where E is the projectile energy. The data are presented in scientific notation, with characteristics shown in square brackets (i.e., $1.28[6]\equiv 1.28\times 10^6$).

θ (degrees)	$\frac{d\sigma(\theta)}{d\Omega}$ (Å^2/sr) $E=500$ eV	$E=1500$ eV	$E=5000$ eV
0.048±0.007	1.28±0.07[6]	1.33±0.07[6]	4.64±0.28[5]
0.055±0.007	1.07±0.06[6]	7.92±0.42[5]	4.23±0.23[5]
0.062±0.007	8.31±0.44[5]	4.61±0.26[5]	3.28±0.18[5]
0.070±0.007	5.92±0.33[5]	2.79±0.17[5]	2.71±0.15[5]
0.077±0.007	4.34±0.25[5]	1.81±0.13[5]	2.08±0.11[5]
0.085±0.007	3.06±0.19[5]	1.26±0.10[5]	1.62±0.09[5]
0.092±0.008	2.08±0.14[5]	1.25±0.09[5]	1.45±0.08[5]
0.099±0.008	1.30±0.11[5]	1.36±0.10[5]	1.26±0.07[5]
0.107±0.008	9.92±0.87[4]	1.27±0.09[5]	1.09±0.06[5]
0.114±0.008	5.77±0.65[4]	1.20±0.08[5]	9.64±0.57[4]
0.121±0.008	5.90±0.63[4]	9.98±0.72[4]	8.22±0.51[4]
0.125±0.017		9.31±0.52[4]	7.74±0.38[4]
0.129±0.008	5.17±0.62[4]	8.04±0.60[4]	7.22±0.45[4]
0.136±0.008	6.02±0.67[4]	7.16±0.55[4]	6.31±0.40[4]
0.143±0.008	5.52±0.66[4]	5.11±0.46[4]	5.63±0.36[4]
0.151±0.008	4.48±0.64[4]	5.36±0.44[4]	5.03±0.33[4]
0.154±0.018	5.75±0.31[4]	5.02±0.31[4]	5.03±0.25[4]
0.158±0.008	5.50±0.64[4]	4.56±0.40[4]	4.20±0.30[4]
0.184±0.018	4.38±0.24[4]	3.69±0.24[4]	3.29±0.18[4]
0.213±0.018	2.58±0.17[4]	2.65±0.18[4]	2.47±0.13[4]
0.243±0.018	1.94±0.13[4]	1.93±0.14[4]	1.97±0.11[4]
0.272±0.019	1.67±0.12[4]	1.60±0.12[4]	1.45±0.08[4]
0.301±0.019	1.43±0.11[4]	1.05±0.10[4]	1.26±0.07[4]
0.331±0.020	9.92±0.87[3]	8.53±0.85[3]	1.09±0.06[4]
0.360±0.020	8.86±0.81[3]	7.96±0.74[3]	8.79±0.53[3]
0.390±0.021	8.01±0.74[3]	6.35±0.65[3]	7.25±0.46[3]
0.419±0.021	7.82±0.72[3]	5.28±0.60[3]	6.44±0.41[3]
0.448±0.022	5.78±0.65[3]	4.59±0.53[3]	5.86±0.38[3]
0.478±0.022	5.70±0.64[3]	4.40±0.50[3]	5.26±0.35[3]
0.507±0.023	5.15±0.60[3]	3.90±0.48[3]	4.33±0.30[3]

analysis technique has been presented by Nitz *et al.*[1] and only a brief review will be provided here. Data are accumulated until the statistical uncertainty in the signal at a given angle is small, typically less than 10%. Two data sets, one with gas in the target cell and one without, are taken. This procedure permits discrimination between counts due to scattering from the target gas and counts arising from other sources, such as scattering from the background gas, scattering from edges of apertures, and dark counts. The scattered flux, $\Delta S(\theta)$, is obtained by organizing the 90×90 data arrays into concentric rings and subtracting the gas-out data from the gas-in data.

The experimental uncertainty in the number of counts at a particular angle is primarily statistical, while the angular uncertainty arises from the finite width of the primary neutral beam, the discrete nature of the analysis rings, and electronic noise in the detector's position encoding circuits. Factors contributing to the experimental uncertainties are summarized in Table I.

III. RESULTS AND DISCUSSION

Differential cross sections have been obtained at projectile energies of 0.5, 1.5, and 5.0 keV and the results are presented in Tables II–V. The 0.5-keV data are plotted in Figs. 2–5, along with DCS's calculated from various interaction potentials.

The plotted cross sections each show an undulation at about 0.1°, superimposed on a monotonically decreasing curve. Beier[3] explains this undulation as the quantum-mechanical analogue of optical Fraunhofer diffraction; the matter wave of the projectile is diffracted by the target atom. Calculations by Nitz *et al.*[1] for He-He scattering demonstrate that this structure arises normally in quantum-mechanical calculations of scattering from a steeply rising, lower repulsive wall of an interaction potential. The undulation has been observed previously in absolute He-He measurements by Nitz *et al.*[1] and in relative cross-section measurements by Leonas and Sermyagin.[6] Several authors[3,7] have calculated differential cross sections for scattering in this angular range and their results are consistent with the present observations.

Over the years, information about the He–rare-gas interaction potentials has been pieced together from a combination of experiment and theory, and a number of analytic forms for the potentials have been derived. In a comprehensive review by Aziz,[4] the Hartree-Fock dispersion (HFD) results of Buck[8] are recommended for

TABLE III. Laboratory frame differential cross sections, $d\sigma(\theta)/d\Omega$, for He + Ar collisions, where E is the projectile energy.

θ (degrees)	$\frac{d\sigma(\theta)}{d\Omega}$ (Å^2/sr) $E=500$ eV	$E=1500$ eV	$E=5000$ eV
0.048±0.007	2.29±0.12[6]	1.22±0.06[6]	8.04±0.43[5]
0.055±0.007	1.72±0.09[6]	5.73±0.31[5]	6.49±0.33[5]
0.062±0.007	1.25±0.07[6]	3.87±0.21[5]	4.55±0.23[5]
0.070±0.007	7.27±0.43[5]	3.78±0.20[5]	3.59±0.19[5]
0.077±0.007	4.49±0.30[5]	3.60±0.18[5]	2.96±0.15[5]
0.085±0.007	2.77±0.21[5]	3.45±0.17[5]	2.60±0.14[5]
0.092±0.008	1.57±0.15[5]	2.63±0.14[5]	2.18±0.12[5]
0.099±0.008	1.33±0.13[5]	2.18±0.12[5]	1.90±0.10[5]
0.107±0.008	1.28±0.12[5]	1.74±0.09[5]	1.73±0.09[5]
0.114±0.008	1.36±0.12[5]	1.42±0.08[5]	1.42±0.08[5]
0.121±0.008	1.24±0.12[5]	1.33±0.07[5]	1.21±0.07[5]
0.125±0.017		1.23±0.06[5]	1.29±0.06[5]
0.129±0.008	1.36±0.12[5]	1.22±0.07[5]	1.15±0.06[5]
0.136±0.008	1.34±0.11[5]	1.13±0.06[5]	1.08±0.06[5]
0.143±0.008	1.21±0.11[5]	9.97±0.57[4]	9.60±0.55[4]
0.151±0.008	9.33±1.00[4]	8.60±0.51[4]	8.88±0.51[4]
0.154±0.018	8.89±0.50[4]	8.35±0.40[4]	8.46±0.41[4]
0.158±0.008	8.75±0.98[4]	8.34±0.49[4]	8.27±0.49[4]
0.184±0.018	5.23±0.33[4]	5.89±0.29[4]	6.11±0.30[4]
0.213±0.018	4.32±0.28[4]	3.93±0.20[4]	4.43±0.23[4]
0.243±0.018	3.63±0.25[4]	3.01±0.16[4]	3.36±0.17[4]
0.272±0.019	2.60±0.19[4]	2.61±0.14[4]	2.67±0.14[4]
0.301±0.019	2.06±0.17[4]	2.09±0.11[4]	2.02±0.11[4]
0.331±0.020	1.99±0.16[4]	1.74±0.09[4]	1.54±0.09[4]
0.360±0.020	1.66±0.15[4]	1.40±0.08[4]	1.09±0.06[4]
0.390±0.021	1.47±0.14[4]	1.23±0.07[4]	8.73±0.55[3]
0.419±0.021	1.15±0.13[4]	1.07±0.06[4]	6.74±0.46[3]
0.448±0.022	9.77±1.17[3]	8.70±0.54[3]	5.40±0.40[3]
0.478±0.022	9.44±1.11[3]	8.67±0.52[3]	4.66±0.36[3]
0.507±0.023	8.17±1.12[3]	7.48±0.47[3]	3.19±0.30[3]

He-Ne. In addition, Aziz[9] has provided recent HFD potentials for He-Ar, He-Kr, and He-Xe. None of these results are obtained *a priori;* in all cases the calculations are normalized to experimental results. The data used for normalization are obtained from thermal-energy gas-phase experiments involving relatively small interaction energies. The potentials derived should therefore be most applicable for larger (typically > 2.0 Å) internuclear separations and are most accurate in the region of the attractive well. The only significantly different procedure was that employed by Foreman, Lee, and Rol[10] (FLR) who determined Born-Mayer potentials over the internuclear range of 1–2.5 Å by formally inverting their measured keV-energy total scattering cross sections.

In order to test the validity of different potentials in the range of scattering angles relevant to the present work, a semiclassical, partial-wave method was used to numerically determine DCS's from each potential. Details of the computation are given in the appendix of Nitz *et al.*[1] The transformation between center of mass and lab angles is given by[11]

$$\tan\theta_{\rm lab}=\frac{\sin\theta_{\rm c.m.}}{\cos\theta_{\rm c.m.}+\rho} ,$$

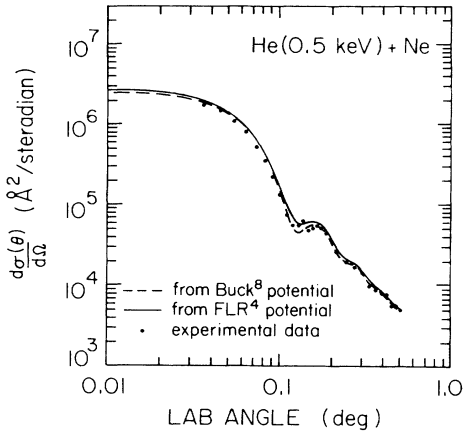

FIG. 2. Differential cross sections for He-Ne scattering at a projectile energy of 0.5 keV.

where $\rho \equiv m_P/m_T$ is the ratio of the projectile and target masses. The theoretical results have been transformed into the laboratory frame by use of the equation

$$\left[\frac{d\sigma(\theta_{\rm lab})}{d\Omega}\right]_{\rm lab}=\left[\frac{d\sigma(\theta_{\rm c.m.})}{d\Omega}\right]_{\rm c.m.}\frac{(1+2\rho\cos\theta+\rho^2)^{3/2}}{1+\rho\cos\theta}$$

TABLE IV. Laboratory frame differential cross sections, $d\sigma(\theta)/d\Omega$, for He + Kr collisions, where E is the projectile energy.

θ (degrees)	$\frac{d\sigma(\theta)}{d\Omega}$ (Å^2/sr) $E=500$ eV	$E=1500$ eV	$E=5000$ eV
0.048±0.007	2.83±0.14[6]	1.19±0.06[6]	1.03±0.05[6]
0.055±0.007	1.97±0.10[6]	5.78±0.31[5]	7.02±0.35[5]
0.062±0.007	1.35±0.07[6]	4.59±0.25[5]	5.28±0.27[5]
0.070±0.007	8.12±0.44[5]	4.83±0.25[5]	4.22±0.22[5]
0.077±0.007	4.39±0.27[5]	4.47±0.23[5]	3.66±0.19[5]
0.085±0.007	2.75±0.18[5]	3.44±0.18[5]	2.93±0.15[5]
0.092±0.008	2.20±0.16[5]	2.75±0.15[5]	2.46±0.13[5]
0.099±0.008	1.95±0.14[5]	2.06±0.11[5]	2.16±0.12[5]
0.107±0.008	1.91±0.13[5]	1.76±0.10[5]	1.83±0.10[5]
0.114±0.008	2.05±0.14[5]	1.63±0.09[5]	1.68±0.09[5]
0.121±0.008	2.00±0.13[5]	1.46±0.08[5]	1.43±0.08[5]
0.125±0.017		1.33±0.06[5]	1.28±0.06[5]
0.129±0.008	2.14±0.14[5]	1.41±0.08[5]	1.24±0.07[5]
0.136±0.008	1.60±0.11[5]	1.18±0.07[5]	1.10±0.06[5]
0.143±0.008	1.25±0.09[5]	1.07±0.06[5]	9.64±0.59[4]
0.151±0.008	1.03±0.09[5]	9.48±0.60[4]	9.83±0.62[4]
0.154±0.018	9.60±0.51[4]	8.55±0.42[4]	8.72±0.43[4]
0.158±0.008	8.32±0.81[4]	8.38±0.55[4]	8.09±0.52[4]
0.184±0.018	6.73±0.37[4]	6.12±0.30[4]	5.88±0.29[4]
0.213±0.018	5.07±0.30[4]	4.54±0.23[4]	4.56±0.23[4]
0.243±0.018	4.06±0.25[4]	3.46±0.18[4]	3.25±0.17[4]
0.272±0.019	3.05±0.20[4]	2.64±0.14[4]	2.39±0.13[4]
0.301±0.019	2.47±0.17[4]	2.24±0.12[4]	1.74±0.10[4]
0.331±0.020	2.10±0.15[4]	1.88±0.10[4]	1.44±0.08[4]
0.360±0.020	1.66±0.14[4]	1.59±0.09[4]	1.14±0.07[4]
0.390±0.021	1.55±0.12[4]	1.39±0.08[4]	9.32±0.59[3]
0.419±0.021	1.33±0.11[4]	1.11±0.07[4]	7.41±0.50[3]
0.448±0.022	1.12±0.11[4]	1.04±0.06[4]	5.89±0.43[3]
0.478±0.022	9.89±0.99[3]	8.21±0.53[3]	5.35±0.39[3]
0.507±0.023	8.42±0.98[3]	8.22±0.52[3]	3.78±0.34[3]

TABLE V. Laboratory frame differential cross sections, $d\sigma(\theta)/d\Omega$ for He + Xe collisions, where E is the projectile energy.

θ (degrees)	$\frac{d\sigma(\theta)}{d\Omega}$ (Å^2/sr) $E=500$ eV	$E=1500$ eV	$E=5000$ eV
0.048±0.007	3.32±0.15[6]	1.10±0.06[6]	1.18±0.06[6]
0.055±0.007	2.19±0.10[6]	6.98±0.37[5]	8.52±0.42[5]
0.062±0.007	1.35±0.06[6]	6.44±0.32[5]	6.29±0.31[5]
0.070±0.007	7.37±0.36[5]	6.37±0.31[5]	5.15±0.26[5]
0.077±0.007	4.19±0.22[5]	5.07±0.25[5]	4.28±0.22[5]
0.085±0.007	2.76±0.15[5]	4.15±0.21[5]	3.66±0.19[5]
0.092±0.008	2.61±0.14[5]	2.98±0.16[5]	3.01±0.15[5]
0.099±0.008	2.65±0.14[5]	2.41±0.13[5]	2.70±0.14[5]
0.107±0.008	2.78±0.14[5]	2.30±0.12[5]	2.14±0.11[5]
0.114±0.008	2.53±0.13[5]	2.07±0.11[5]	1.91±0.10[5]
0.121±0.008	2.41±0.13[5]	1.83±0.10[5]	1.68±0.09[5]
0.125±0.017		1.59±0.07[5]	1.56±0.07[5]
0.129±0.008	1.99±0.11[5]	1.68±0.09[5]	1.51±0.08[5]
0.136±0.008	1.74±0.09[5]	1.39±0.08[5]	1.24±0.07[5]
0.143±0.008	1.33±0.08[5]	1.24±0.07[5]	1.14±0.06[5]
0.151±0.008	1.14±0.07[5]	1.16±0.07[5]	9.92±0.58[4]
0.154±0.018	1.04±0.05[5]	1.03±0.05[5]	9.68±0.46[4]
0.158±0.008	8.88±0.60[4]	1.09±0.07[5]	9.66±0.58[4]
0.184±0.018	7.99±0.42[4]	7.07±0.34[4]	6.58±0.32[4]
0.213±0.018	5.51±0.31[4]	5.49±0.27[4]	4.56±0.23[4]
0.243±0.018	4.55±0.26[4]	4.07±0.20[4]	3.24±0.17[4]
0.272±0.019	3.35±0.20[4]	3.27±0.17[4]	2.47±0.13[4]
0.301±0.019	3.01±0.19[4]	2.70±0.14[4]	1.92±0.10[4]
0.331±0.020	2.37±0.16[4]	2.25±0.12[4]	1.34±0.08[4]
0.360±0.020	2.01±0.14[4]	1.83±0.10[4]	1.11±0.07[4]
0.390±0.021	1.93±0.13[4]	1.60±0.09[4]	9.16±0.58[3]
0.419±0.021	1.60±0.12[4]	1.43±0.08[4]	7.34±0.49[3]
0.448±0.022	1.23±0.11[4]	1.22±0.07[4]	5.67±0.42[3]
0.478±0.022	1.35±0.11[4]	1.14±0.06[4]	5.25±0.38[3]
0.507±0.023	1.03±0.10[4]	1.05±0.06[4]	4.66±0.36[3]

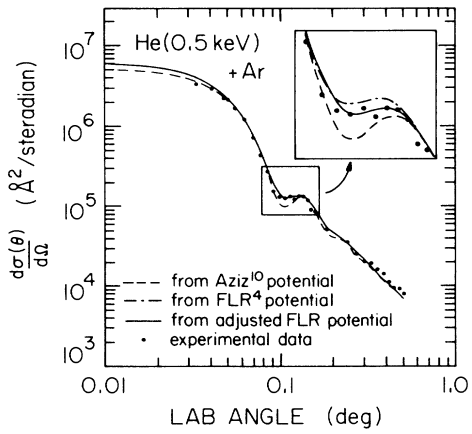

FIG. 3. Differential cross sections for He-Ar scattering at a projectile energy of 0.5 keV.

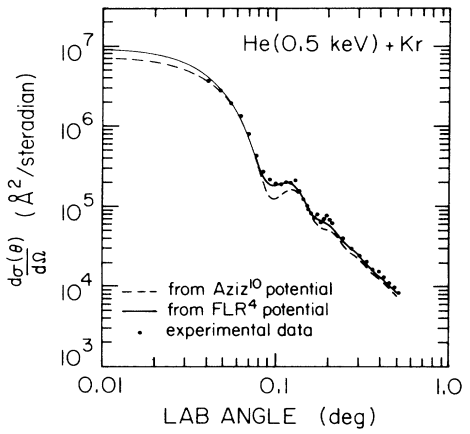

FIG. 4. Differential cross sections for He-Kr scattering at a projectile energy of 0.5 keV.

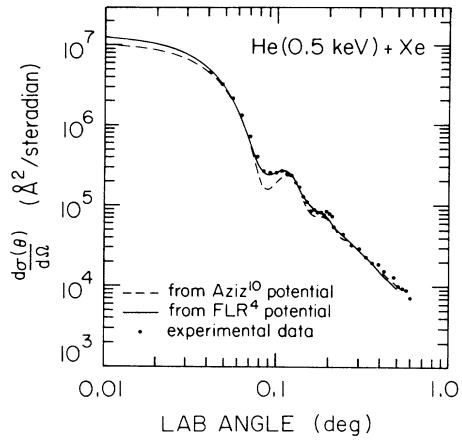

FIG. 5. Differential cross sections for He-Xe scattering at a projectile energy of 0.5 keV.

TABLE VI. Parameters for the Born-Mayer potential (Ref. 10), $V(r)=Ae^{-\alpha r}$, for He-Ne, He-Ar, He-Kr, and He-Xe. The semiclassical phase shifts are used to determine the deflection function $\theta(l)=2d\delta_l/dl$. The potentials are considered valid over the range $r_L \leqq r \leqq r_u$ where r_L is the distance of closest approach for scattering at the maximum observed angle and r_U is the corresponding quantity for the minimum angle.

	A (eV)	α (Å^{-1})	r_L (Å)	r_U (Å)
He-Ne[a]	788	4.356	1.4	2.0
He-Ar[b]	492	3.443	1.7	2.4
He-Kr[c]	856	3.339	1.9	2.7
He-Xe[c]	932	3.137	2.0	2.9

[a]Foreman, Lee, and Rol, private communication cited by Aziz (Ref. 4).
[b]FLR potential with A reduced by 20%.
[c]FLR potentials with A increased by 20%.

for direct comparison to the experimental data. The cross sections calculated for He-Ne using the HFD potential are virtually identical to those derived from the FLR potential, and for He-Ne, Kr, and Xe the FLR potentials give DCS's that are very close to the measured data. The HFD potentials lead to deeper undulations than those of the measured cross sections.

The effect of the finite angular resolution of the apparatus was estimated by calculating the convolution of the theoretical cross sections with a well-characterized apparatus function which accounts for the discrete analysis rings, the physical beam size, and the inherent PSD position-finding uncertainty. The convolved cross sections differ only slightly from those without convolution, even where the cross section is changing rapidly. The data for all reactions lie closer to the convolved FLR results than to the convolved HFD results.

Although the FLR results agree very well with the present experimental results, even better agreement may in some cases be obtained by appropriate adjustment of either the amplitude or the exponential factor of the FLR potential. Figures 2–5 show the DCS's calculated from the unmodified FLR potentials and from the HFD potentials. A further calculation for He-Ar is shown in the inset of Fig. 3, where the amplitude of the FLR potential has been reduced by 20% to give the best fit to the present data. Better fits to the He-Kr and He-Xe data are obtained by increasing the amplitude of the FLR potential by 20%. The parameters for potentials giving DCS's in best agreement with the present measurements are listed in Table VI.

IV. SUMMARY

Absolute differential cross sections for He-Ne, Ar, Kr, and Xe neutral scattering at projectile energies of 0.5, 1.5, and 5.0 keV have been measured over the angular range 0.05°–0.5°. The results have been used to evaluate candidate potentials proposed for the He–rare-gas systems. In several cases, candidate potentials have been adjusted slightly to provide model cross sections that agree more closely with experimental results.

ACKNOWLEDGMENTS

The authors wish to thank R. A. Aziz for providing his unpublished potentials. They further wish to acknowledge productive discussions with J. H. Newman, N. F. Lane, and S. Estreicher, and assistance in the initial data collection by C. Chitnis. This work was supported by Welch Foundation Grant No. C-552, by NSF Grant No. ATM-8411853, and by Saint Olaf College through its sabbatical leave program.

*Present address: Physics Department, Saint Olaf College, Northfield, MN 55057.

[1]D. E. Nitz, R. S. Gao, L. K. Johnson, K. A. Smith, and R. F. Stebbings, Phys. Rev. A **35**, 4541 (1987).
[2]J. H. Newman, K. A. Smith, R. F. Stebbings, and Y. S. Chen, J. Geophys. Res. **90**, 11045 (1985).
[3]H. J. Beier, J. Phys. B **6**, 683 (1973).
[4]R. A. Aziz, in *Inert Gases*, edited by M. L. Klein (Springer-Verlag, Berlin, 1984), Vol. 34, Chap. 2.
[5]R. S. Gao, P. S. Gibner, J. H. Newman, K. A. Smith, and R. F. Stebbings, Rev. Sci. Instrum. **55**, 1756 (1984).
[6]V. B. Leonas and A. V. Sermyagin, Khim. Vys. Energ. **11**, 296 (1977).
[7]E. A. Mason, J. T. Vanderslice, and C. J. G. Raw, J. Chem. Phys. **40**, 2153 (1964); R. J. Munn, E. A. Mason, and F. J. Smith, *ibid.* **41**, 3978 (1964); F. J. Smith, E. A. Mason, and J. T. Vanderslice, *ibid.* **42**, 3257 (1965); M. V. Berry, J. Phys. B **2**, 381 (1969); K. E. Mount, *ibid.* **6**, 1397 (1973).
[8]U. Buck (unpublished), as discussed in Aziz (Ref. 4).
[9]R. A. Aziz (private communication).
[10]P. B. Foreman, A. B. Lee, and P. K. Rol (unpublished), as discussed in Aziz (Ref. 4).
[11]H. Goldstein, *Classical Mechanics*, 2nd ed. (Addison-Wesley, Reading, MA, 1981), pp. 116–117.